Biomaterials 35 (2014) 3188–3197

Contents lists available at ScienceDirect

Biomaterials

journal homepage: www.elsevier.com/locate/biomaterials

Engineering hybrid polymer-protein super-aligned nanofibers via rotary jet spinning☆

Mohammad R. Badrossamay [a,b,1], Kartik Balachandran [a,b,1], Andrew K. Capulli [a,b], Holly M. Golecki [a,b], Ashutosh Agarwal [a,b], Josue A. Goss [a,b], Hansu Kim [c], Kwanwoo Shin [c], Kevin Kit Parker [a,b,*]

[a] Disease Biophysics Group, School of Engineering and Applied Sciences Harvard University, 60 Oxford St, Cambridge, MA 02138, USA
[b] Wyss Institute for Biologically Inspired Engineering, Harvard University, 3 Blackfan Cir, Boston, MA 02115, USA
[c] Department of Chemistry and Sogang-Harvard Center for Disease Biophysics Research, 35 Baekbeom-ro, Mapo-gu, Seoul 121-742, South Korea

ARTICLE INFO

Article history:
Received 25 November 2013
Accepted 20 December 2013
Available online 20 January 2014

Keywords:
Biomedical applications
Jet spinning
Nanofiber scaffold
Polymer-protein hybrid
Tissue engineering

ABSTRACT

Cellular microenvironments are important in coaxing cells to behave collectively as functional, structured tissues. Important cues in this microenvironment are the chemical, mechanical and spatial arrangement of the supporting matrix in the extracellular space. In engineered tissues, synthetic scaffolding provides many of these microenvironmental cues. Key requirements are that synthetic scaffolds should recapitulate the native three-dimensional (3D) hierarchical fibrillar structure, possess biomimetic surface properties and demonstrate mechanical integrity, and in some tissues, anisotropy. Electrospinning is a popular technique used to fabricate anisotropic nanofiber scaffolds. However, it suffers from relatively low production rates and poor control of fiber alignment without substantial modifications to the fiber collector mechanism. Additionally, many biomaterials are not amenable for fabrication via high-voltage electrospinning methods. Hence, we reasoned that we could utilize rotary jet spinning (RJS) to fabricate highly aligned hybrid protein-polymer with tunable chemical and physical properties. In this study, we engineered highly aligned nanofiber constructs with robust fiber alignment from blends of the proteins collagen and gelatin, and the polymer poly-ε-caprolactone via RJS and electrospinning. RJS-spun fibers retain greater protein content on the surface and are also fabricated at a higher production rate compared to those fabricated via electrospinning. We measured increased fiber diameter and viscosity, and decreasing fiber alignment as protein content increased in RJS hybrid fibers. RJS nanofiber constructs also demonstrate highly anisotropic mechanical properties mimicking several biological tissue types. We demonstrate the bio-functionality of RJS scaffold fibers by testing their ability to support cell growth and maturation with a variety of cell types. Our highly anisotropic RJS fibers are therefore able to support cellular alignment, maturation and self-organization. The hybrid nanofiber constructs fabricated by RJS therefore have the potential to be used as scaffold material for a wide variety of biological tissues and organs, as an alternative to electrospinning.

1. Introduction

Therapeutic tissue engineering aims to produce synthetic tissues and organs to replace diseased and dying tissues and organs in the body [1]. An important component of engineered tissues is the scaffold that provides structural support for *ex vivo* or *in vivo* cell adhesion and tissue regeneration [2,3]. In addition to long-term biocompatibility, the ideal scaffold should effectively mimic the hierarchical three-dimensional architecture of native tissues [4].

Building a fiber-based scaffold from proteins will provide for a native, biomimetic environment that promotes cell attachment, maturation, differentiation and proliferation [4]; however, protein materials are not always chemically or mechanically robust enough

* Corresponding author. Disease Biophysics Group, Wyss Institute for Biologically Inspired Engineering, School of Engineering and Applied Sciences, Harvard University, 29 Oxford St, Pierce Hall 321, Cambridge, MA 02138, USA.
E-mail address: kkparker@seas.harvard.edu (K.K. Parker).

[1] M. R. Badrossamay and K. Balachandran contributed equally to this work.

0142-9612/$ – see front matter © 2014 The Authors. Published by Elsevier Ltd. All rights reserved.
http://dx.doi.org/10.1016/j.biomaterials.2013.12.072

for manufacturing and use [5–7]. Chemical crosslinking can stabilize protein structure and prevent hydrolysis under physiological conditions, but often promotes inflammation, calcification and tissue rejection [8,9]. Recent work has focused on utilizing protein-polymer hybrid composites as scaffold materials with tunable properties, the polymer component imparting mechanical strength, forming the structural backbone of the scaffold [6,10]. These reports on protein-polymer hybrids utilized electrospinning, which despite its versatility, has poor control over fiber orientation and relatively low production rates using high voltages [11–14]. Additionally, some materials are not easily fabricated into nanofibrous structures using conventional electrospinning methods due to high curing temperature [15] and low solution viscosity [16]. Thus, we need an alternative method for reproducible fabrication of hybrid nanofiber scaffolds that is able to overcome these limitations of electrospinning.

We hypothesized that we could synthesize highly anisotropic protein-polymer hybrid nanofibers by modifying the rotary jet spinning (RJS) method for producing nanofibers [11,17]. RJS is a technique that utilizes high-speed rotating polymer solution jets to extrude three-dimensional nanofiber structures with highly aligned nanofibers. Poly-ε-caprolactone (PCL), a biodegradable polyester with low glass transition temperature that degrades via hydrolysis of its ester linkages in physiological conditions, was utilized as the synthetic component [18,19]. However, PCL-based scaffolds lack the ability to interact with cells and to support cell adhesion and migration. Collagen, the most abundant structural protein found in mammals [20], or its hydrolyzed form, gelatin, made up the protein components of the hybrid material. Similar polymer/protein hybrid electrospun scaffolds have shown promise as tissue engineering materials demonstrating favorable mechanical properties and cellular adhesion [21–23]. However, electrospun fibers lack a high degree of fiber alignment and have relatively low production rates (~1 ml/h). Our study objective was therefore to engineer protein-polymer biohybrid aligned nanofibers via RJS and characterize their physical, chemical and biomimetic properties. We also highlight key physical and chemical differences in electrospun and RJS fabricated biohybrid nanofibers.

2. Materials and methods

2.1. Polymer materials

PCL (Mn 70,000–90,000; Sigma–Aldrich, St. Louis, MO), gelatin Type A (~300 Bloom; Sigma–Aldrich) and solvent 1,1,1,3,3,3-Hexafluoro-2-propanol (HFIP; Sigma–Aldrich) were used as received without further modifications. Collagen Type I (Sigma–Aldrich) was obtained as a 4 mg/mL solution in 20 mM acetic acid and lyophilized using standardized protocols before use.

2.2. Fabrication of protein-polymer hybrid SANF scaffolds via rotary jet spinning

PCL, PCL-collagen and PCL-gelatin fibers with different compositions were fabricated using rotary jet spinning (RJS). Briefly, PCL/collagen (75:25), PCL/gelatin (75:25, 50:50, 25:75) and PCL were dissolved in HFIP at various mass ratios at 6% total dopant concentration (w/v). Pure protein SANF scaffolds were not fabricated in this study due to their instability in an aqueous environment without glutaraldehyde fixation. This solution was injected into the rotating reservoir (~30,000 rpm) of the RJS system and fibers were collected proximal to the high-speed rotating reservoir. The scaffolds were spun for approximately 2 min for each condition and dried overnight in a desiccator to remove excess solvent prior to use.

2.3. Fabrication of protein-polymer hybrid scaffolds via electrospinning

PCL/collagen (75:25) was dissolved in HFIP at 6% total concentration (w/v). The solution was placed in a 1 mL syringe with a stainless steel needle (23.5 gauge), attached to a syringe pump (100 Series, Kd Scientific, USA) at a flow rate of 0.08 mL/h. A grounded copper plate was placed on 10 cm from the end of the needle and 14 kV of electrical potential was applied by high-voltage supplier (HV30, NanoNC, Korea) to generate the required potential difference between the tip of the needle to collector to produce fibers.

2.4. Scanning electron microscopy and physical characterization

Fiber diameter and alignment were characterized using a field emission scanning electron microscope (FESEM; Carl Zeiss, Dresden, Germany). Briefly, bare fiber samples were removed from the collector, mounted on sample stubs and sputter coated with Pt/Pd (Denton Vacuum, Moorestown, NJ). Samples that were seeded with cells were first fixed in a 2.5% (v/v) solution of glutaraldehyde in 0.1 M sodium cacodylate buffer (Electron Microscopy Sciences, Hatfield, PA) for 2 h. The samples were then washed 3 times in buffer and dehydrated with increasing concentrations of absolute ethanol (50%, 75%, 90% (2×), 100% (2×)). In place of critical point drying that can induce artifacts in biological samples [24], specimens were dried in hexamethyldisilazane (Electron Microscopy Sciences) via serial exchange from the ethanol (100:0, 50:50, 0:100) and sputter coated as before. Images were acquired and analyzed using ImageJ software (National Institutes of Health, Bethesda, MD). A total of 100–300 fibers were analyzed (5 random fields of view per sample) to determine the fiber diameter. At least 8 fields of view were analyzed per sample for fiber alignment/orientation. Fiber alignment was characterized using a parameter termed orientation order parameter (OOP). The OOP was developed for the study of organization of liquid crystals [25] and adapted for biological applications [26], and was computed from the pixel-based orientation vectors of the fiber images (Supplementary Fig. 1). The parameter value ranges from zero in isotropic systems to one in perfectly aligned systems.

2.5. Viscosity measurements

Rheological measurements were made on freshly prepared PCL and PCL/gelatin solutions of varying ratios (Supplementary Fig. 1). Solutions were loaded into the viscometer (Model AR-G2, TA instruments, New Castle, DE) fitted with a standard-size 40 mm cone and plate geometry. Viscosities were measured under steady state shear rate from 0.1 to 1000 s^{-1}. Experimental viscosity versus polymer concentration curve is best fitted by a polynomial function for small concentrations of polymer and by an exponential function at higher concentrations.

2.6. Chemical characterization

Attenuated Total Reflectance-Fourier Transform Infrared (ATR-FTIR) spectroscopy of PCL, PCL/collagen and PCL/gelatin scaffolds was obtained on a Nicolet ECO 1000 spectrometer system (Pittsburgh, PA) over a range of 4000–600 cm^{-1} at a resolution of 1 cm^{-1}. X-Ray Diffraction (XRD) was measured on a Scintag XDS 2000 (Cupertino, CA) instrument with Cu Ka radiation (1.54 nm wavelength) at 0.25° increments using fibers deposited on quartz substrate to examine the crystal structure of SANF scaffolds. Differential Scanning Calorimetry (DSC) was measured on a TA Q2000 instrument (New Castle, DE) to analyze polymer and hybrid melting and recrystallization temperatures. Fourier Transform Infrared spectroscopy imaging (imaging IR) of PCL, PCL/collagen, and collagen scaffolds was obtained on a Varian 640 FTIR spectrometer and a Varian 620 imaging microscope (Palo Alto, CA) equipped with a liquid nitrogen cooled 16 × 16 pixel focal plane array (FPA) detector. Imaging IR data were collected at a resolution of 4 cm^{-1} over a range of 4000–900 cm^{-1} using 64× scanning; scaffold samples were mounted on gold coated wafers (Sigma–Aldrich). Polymer/protein hybrid electrospun and RJS scaffolds were soaked in distilled water. Every 24 h, a portion of soaked fibers were taken out of water and dried in the oven at 37 °C for 12 h before being imaged by FTIR to quantify the time rate of change of protein composition on the fiber surface.

2.7. Mechanical characterization

Mechanical characterization of the SANF scaffolds was performed using an Instron 5542 mechanical tester (Norwood, MA). Scaffolds were cut into a rectangular shape (5 × 15 mm) and inserted into the grips within a phosphate buffered saline bath heated to 37 °C. Specimens were allowed to equilibrate in the bath under no tension for 15 min, were preconditioned to 3% of original specimen length for 20 cycles, and pulled to failure at 1 mm/min extension rate. At least four specimens from each hybrid composition were tested. Young's modulus (E) was calculated based on the tangent of the stress-strain curve at 0% strain. Ultimate tensile strength (UTS) was also reported.

2.8. Biodegradation analysis [27,28]

Primary neonatal rat fibroblasts were seeded on Transwell® membrane plates (BD Biosciences, San Jose, CA) within 6-well plates that contained PCL, PCL/collagen and PCL/gelatin SANF scaffolds (Supplemental Fig. 3A). Samples were extracted at 0, 2, 7, 14, and 28 days, dried and had their weight measured. Samples were also processed for ATR-FTIR analysis as before. PCL/collagen samples at 0 and 56 days were also processed for SEM analysis to measure fiber diameter, as outlined earlier.

2.9. Cell culture

Neonatal rat ventricular cardiomyocytes, fibroblasts and cortical neurons were isolated from 2-day old Sprague–Dawley rats as previously described [29,30]. Valve interstitial cells (VICs) were a kind gift from the laboratories of Drs. Robert A. Levine and Joyce Bischoff (Massachusetts General Hospital and Children's Hospital Boston, Boston, MA). All procedures were approved by the Harvard Animal Care and Use

Committee. All cells were seeded onto the nanofiber scaffolds at a density of 50,000 cells/cm^2 in appropriate culture medium [30–32] and were incubated for 2–7 days under standard conditions at 37 °C and 5% CO_2.

Following culture, samples were prepared for one of the following analyses. Samples were fixed and prepared for SEM as outlined earlier. SANFs cultured with cardiomyocytes for 5 days were fixed and immunostained for sarcomeric α-actinin. SANFs cultured with neurons for 7 days were fixed and immunostained [30] for neurofilament protein in order to analyze neurite length and branching. Briefly, samples were fixed in 4% paraformaldehyde and 0.05% Triton-X for 15 min, washed in phosphate buffered saline (PBS) and blocked with 5% bovine serum albumin (BSA) in PBS for 30 min at 37 °C. Following blocking, samples were incubated with anti-mouse sarcomeric α-actinin (Sigma) at 1:100 or anti-mouse neurofilament protein (Sigma) at a concentration of 1:100 in 0.5% BSA/PBS for 2 h at room temperature, incubated with appropriate secondary antibody and mounted onto microscope slides using Prolong Gold anti-fade reagent (Invitrogen, Carlsbad, CA). Images were acquired on a Zeiss LSM 510 laser scanning confocal microscope and analyzed using ImageJ software (NIH). At least 8 fields of view were analyzed per sample.

2.10. Cell metabolic activity and injury/death

Samples seeded with VICs were used to assess cell metabolic activity on the different substrates. After 2 and 7 days culture, samples were washed in PBS and incubated with 5 mg/mL MTT reagent in serum free medium (1:10 ratio) for 3 h at 37 °C in 5% CO_2. Medium was extracted from each sample and converted dye was solubilized in 1 mL acidic isopropanol (0.04 M HCl in isopropanol) and vortexed to ensure that the dye dissolved completely. The solution was then transferred to a 96-well plate and read in a plate reader at 570 nm with background subtraction at 650 nm. Cell injury and death was measured via a commercially available lactate dehydrogenase (LDH) cytotoxicity assay (Promega, Fitchburg, WI). Briefly, cardiomyocytes were cultured on SANF scaffolds for 24 h and incubated with conditioned medium using the assay kit for 30 min at 37 °C. Absorbance at 490 nm was measured using a commercially available plate reader. Cells seeded on fibronectin treated PDMS coated glass coverslips served as a comparison.

2.11. Statistical analysis

All data were expressed as mean ± standard error (SEM). Statistical comparisons were done on normally distributed data using analysis of variance (ANOVA) and Tukey's post-hoc tests. ANOVA on ranks followed by Dunn's or Tukey's pairwise comparison was used to analyze data that was not normally distributed. A p-value of less than 0.05 was used as a measure for statistical significance.

3. Results

3.1. Nanofiber fabrication and physical characterization

We have previously fabricated nanofibers with tunable fiber thickness and porosities using RJS [11,17]. In this study, we asked if we could create highly aligned, anisotropic hybrid protein-polymer nanofibers by the same method. For this purpose, we allowed the fibers that collect in the periphery of the collector to wrap around and collect around the rotating reservoir (Fig. 1A; Supplementary Video 1). The rotating reservoir provides tension to the nanofibers, creating densely packed, highly aligned nanofibrous scaffolds that we term super-aligned nanofiber (SANF) constructs (Fig. 1B). These SANF constructs demonstrate robust centimeter (Fig. 1C), millimeter (Fig. 1D), and micrometer scale (Fig. 1E) alignment. The nanofibers were bead-free with narrow diameter distribution. Fiber diameter increased with increasing protein concentration (Fig. 1F).

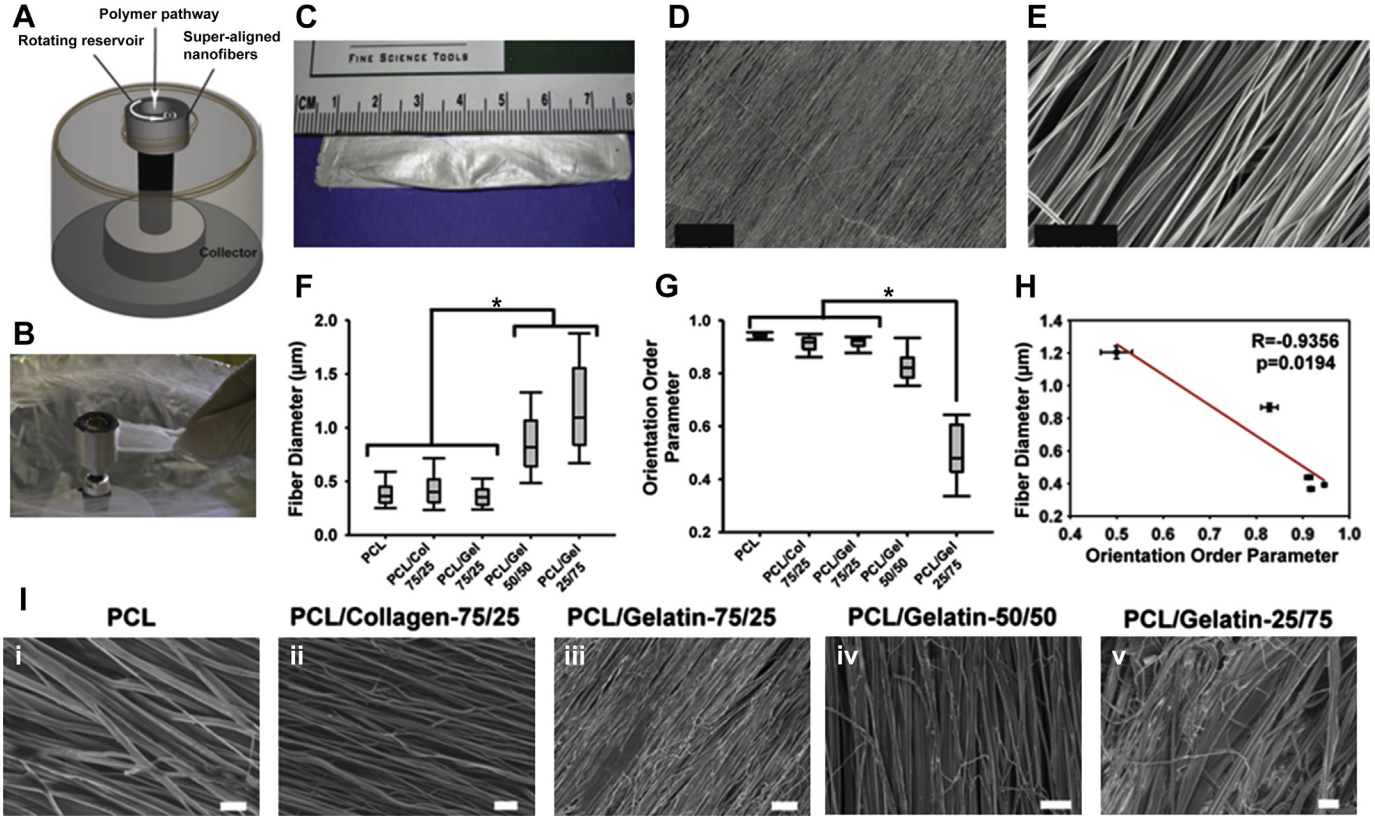

Fig. 1. Method for super-aligned nanofiber (SANF) construct fabrication by RJS. (A) Schematic for RJS fabrication of SANFs. (B) Photograph of collecting SANF constructs from the reservoir. (C) Photographic image of SANF constructs produced by RJS. (D, E) Scanning electron micrograph of SANF constructs in panel C showing fiber alignment from cm to nm scale. Scale bar for (D): 100 μm. Scale bar for (E): 10 μm. (F) Fiber diameter distribution of PCL and PCL/protein hybrid SANF constructs ($N = 8$ samples with 8 fields of view per sample, * = statistical significant difference at $p < 0.05$; box plot: 25–75%, error bars: 10–90%). (G) Orientation order parameter of PCL and PCL/protein hybrid SANF constructs ($N = 9$ different samples with 8 fields of view per sample, * = statistical significant difference at $p < 0.05$; box plot: 25–75%, error bars: 10–90%). (H) Pearson's analysis demonstrating significant negative correlation between fiber diameter and orientation order parameter ($N > 8$). (I) Representative electron micrographs of the SANF constructs demonstrating smaller fibers stretched across the principal fiber direction in samples with higher protein concentration. (Scale bars: Ii – 2 μm; Iii – 10 μm; Iiii – 20 μm; Iiv – 10 μm; Iv – 10 μm).

Median fiber diameter was not significantly different between PCL, PCL/Collagen-75/25, and PCL/Gelatin-75/25 SANFs. Fiber diameter significantly increased as the percentage of protein increased to 50% and 75% (Fig. 1F). PCL/Gelatin-25/75 fibers had a median fiber diameter in excess of 1 micron and therefore require a higher RJS spinning velocity to fabricate nanofibers [11,17].

Supplementary data related to this article can be found online at http://dx.doi.org/10.1016/j.biomaterials.2013.12.072.

We have previously reported a direct correlation with increasing RJS-fiber diameter in with increasing dynamic viscosity [11,17]. In the current study, we applied this technique to blends of synthetic polymers and natural proteins. We report here that the dynamic viscosity of biohybrid solutions increased with increasing protein content (Supplemental Fig. 1D). We have developed a model demonstrating that fiber radius scales as the square root of the kinematic viscosity, ν [17]. This model is in good agreement with our current experimental data (Supplemental Fig 1E), suggesting its utility in predicting the physical properties of polymer/protein biohybrid materials.

We asked if fiber alignment was affected by protein content. We quantified the degree of fiber alignment using the orientation order parameter (OOP), a metric adapted from the field of liquid crystallography (Supplementary Fig. 1A–C) [25,26,33]. Randomly aligned or isotropic fibers have a OOP value of 0 while perfectly aligned fibers have an OOP value of 1. As shown in Fig. 1G, PCL, PCL/Collagen-75/25, and PCL/Gelatin-75/25 SANFs were highly anisotropic with median OOP values greater than 0.85. As protein content increased to 50% and 75%, there was a decreasing trend for the OOP and for PCL/Gelatin-25/75, the OOP was significantly lower with a median value of 0.47 (Fig. 1G). We also noted that fiber alignment was negatively correlated with fiber diameter (Fig. 1H). Representative scanning electron micrographs suggest that the reduction in OOP is due to the presence of thinner fibers that are oriented orthogonally to the primary fiber direction (Fig. 1I). The fiber diameter and viscosity data suggest the relationship between OOP, diameter and viscosity may be due to increased intermolecular attraction with increasing protein content preventing shear-induced slipping of bonds needed to form highly aligned fibers [17].

Thus, these data suggest that we can use the protein/polymer solution viscosity to predict important physical parameters of the final SANF scaffolds – (i) the average fiber diameter and (ii) alignment of the scaffold. Therefore, we can tailor the fiber properties to the desired scaffold architecture.

3.2. Structural conformation and crystallinity of SANF constructs

Structural conformation and crystallinity of an engineered tissue scaffold will influence cell attachment. As a hydrophobic polymer, PCL does not facilitate cellular attachment [19]. We reasoned that the addition of protein into the PCL structure will alter fiber surface properties and secondary structure, and add binding domains for cell attachment, thereby imparting favorable properties for cellular attachment. In order to study the surface characterization, structural configuration and specific intermolecular interactions of hybrid SANF constructs, chemical analysis was performed by attenuated total reflectance-Fourier transform infrared (ATR-FTIR) spectroscopy in the range of 4000–600 cm^{-1}. All characteristic peaks of PCL were observed on PCL SANF scaffolds, including CH_2 stretching (2850–2950 cm^{-1}), carbonyl stretching (1724 cm^{-1}), C–C and C–O stretching in the crystalline phase (1294 cm^{-1}), and the amorphous band of PCL (1161 cm^{-1}) (Supplementary Fig. 2A).

Spectra of PCL/Gelatin and PCL/Collagen SANF constructs show additional peaks in the range of 1500–1800 cm^{-1} when compared to PCL SANFs (Fig. 2A, Supplementary Fig. 2B). These additional bands associated with proteins appeared at approximately

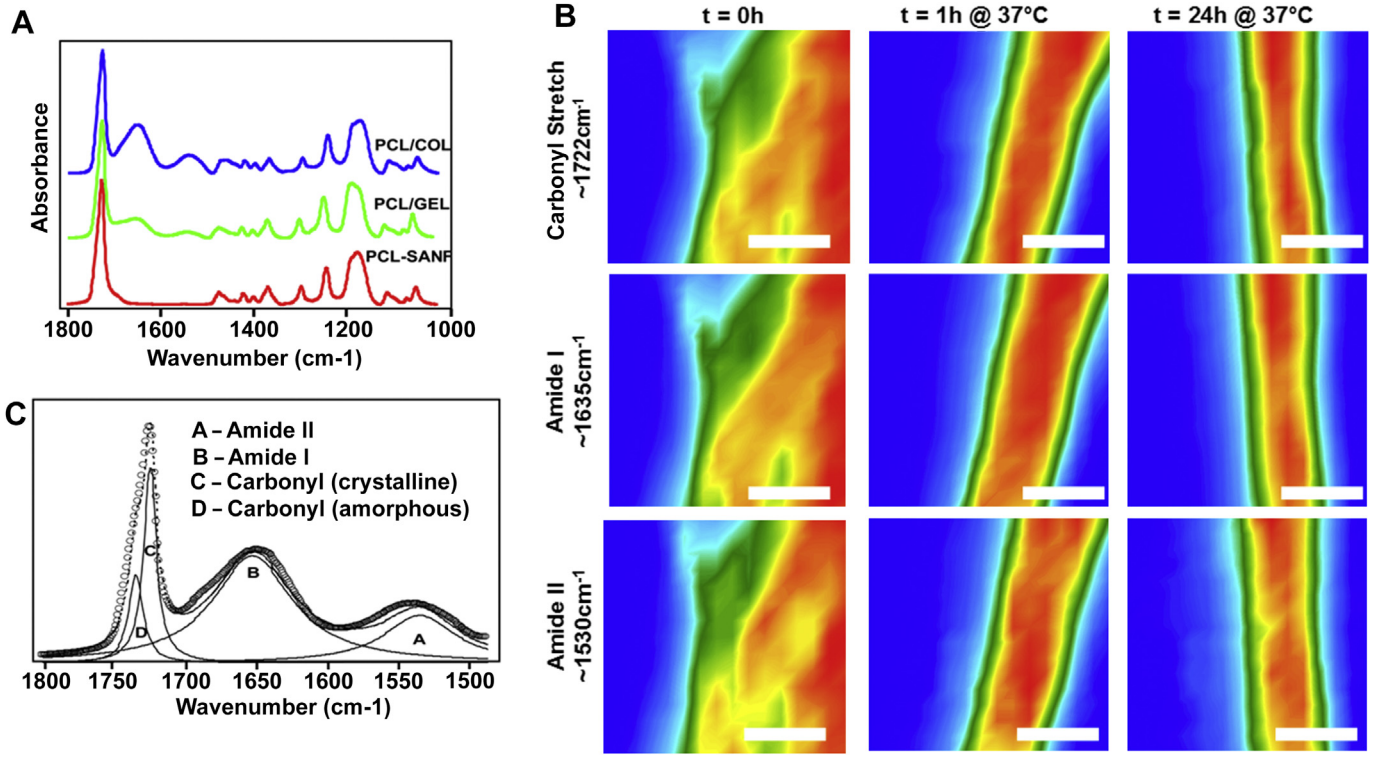

Fig. 2. Chemical and thermal characterization of hybrid constructs (A) ATR-FTIR spectra of PCL SANF, PCL/GEL-SANF and PCL/COL-SANF constructs in the range of 1000–1800 cm^{-1}. (B) Imaging IR of hybrid SANF bundles at $t = 0$, 1, and 24 h. Red represents highest absorbance (thickest portion of the SANF bundle) while blue represents lowest absorbance (Scale bars: 30 μm). (C) Experimental and curve-fitting ATR-FTIR spectra in the range of 1400–1800 cm^{-1} of the PCL/COL-75/25 (open circle: experimental points, broken line: fitting results), A: amide II band, B: amide I band, C: crystalline band of carbonyl, D: amorphous band of carbonyl group.

1650 cm^{-1} (amide I) and 1540 cm^{-1} (amide II) in addition to the peaks of PCL (carbonyl) suggesting altered molecular composition, and incorporation of the protein within the hybrid SANF structure (Supplementary Fig. 2B). Imaging IR data (Fig. 2B) of PCL/collagen biohybrid SANF bundles shows uniform absorbance distribution of both the PCL (carbonyl) and collagen (amide) peaks when dry (post spinning), soaking for 1hr in 37 °C water, and soaking for 24hr in 37 °C water suggesting that the collagen within the PCL/collagen biohybrid structure is relatively stable.

Zeugolis et al. have suggested that electrospinning collagen out of fluoro-alcohol solvents such as HFIP might denature collagen into gelatin [34]. We performed circular dichroism measurements that verify the loss of the helical structure collagen due to HFIP (Supplementary Fig. 2C–D); however, our FTIR data suggest a protective effect of PCL on collagen in the hybrid scaffolds we produced via RJS at the secondary structure level. We note (Supplementary Fig. 2F) that the intensity of the Amide I band in PCL/Collagen-75/25 SANFs is approximately one-quarter that of pure collagen samples, indicative of the reduced quantity of collagen in the sample. The amide I band intensity is decreased markedly in the PCL/Gelatin-75/25 SANFs, and there is also a leftward shift of the intensity of the peak from 1648 cm^{-1} to 1653 cm^{-1}, indicative of denaturation [35,36]. The amide I peak of the PCL/Collagen-75/25 SANF is consistent with pure collagen samples suggesting a protective effect of PCL on the amide bond structure of collagen when the SANFs were prepared using RJS.

The small amorphous band at 1161 cm^{-1} for all SANF constructs suggested that PCL was predominantly crystalline (Supplementary Fig. 2E) [37]. To quantify the change in PCL crystallinity, we analyzed the relative ratios of amorphous (1737 cm^{-1}) to crystalline (1724 cm^{-1}) absorbance of PCL carbonyl stretching within the SANFs [37]. We fit a curve to resolve these peaks within the carbonyl stretching region (1500–1800 cm^{-1}) of the spectra of the SANF constructs (Fig. 2B). Results indicated that the ratio of crystalline to amorphous absorbance values decrease as protein concentration increased (Percent decrease compared to PCL SANFs – PCL/Collagen-75/25: 6.6%; PCL/Gelatin-75/25: 10.3%; PCL/Gelatin-50/50: 12.3%; PCL/Gelatin-25/75: 50.0%).

In order to further confirm that the crystal structure of PCL was conserved during RJS manufacturing of SANF constructs, we performed X-ray diffraction (XRD) analysis, and plotted the data in Fig. 3A. The peak positions for both PCL-chips and PCL SANFs were essentially identical; showing two strong peaks at 21.4° and 23.7°

Table 1
Thermodynamic data of PCL-chips, PCL SANFs, PCL/Gelatin-75/25 SANFs and PCL/COL-75/25 SANFs.

	T_c (°C)	ΔH_c (J/g)	T_m (°C)	ΔH_m (J/g)	Crystallinity (%)
PCL-chips	32.4	56.3	57.3	52.1	37.4
PCL-SANF	41.9	50.1	57.9	52.2	37.4
PCL/GEL-75/25	39.0	27.2	57.4	35.7	34.2
PCL/COL-75/25	34.4, 47.6	14.4, 2.6	55.4	27.2	26.0

attributed to the <110> and <200 > crystallographic directions respectively [38], suggesting no change in crystal structure induced by RJS. There was no significant change in the qualitative diffraction pattern of hybrid constructs when compared to PCL SANFs. However, the diffraction peaks for PCL SANFs were sharper than for hybrid samples, suggesting fewer defects in the crystal structure of the PCL SANFs compared to hybrid SANFs.

3.3. Thermodynamic analysis of SANFs

We used differential scanning calorimetry (DSC) to measure the thermal properties of SANF scaffolds. The crystallization (Fig. 3B) and melting thermograms (Fig. 3C) of PCL SANFs as elucidated via DSC, were identical to PCL-chips indicating no retardation in crystallinity due to the RJS process, in spite of rapid solvent evaporation and elongational stresses [17]. In addition, there was no significant change in the melting temperature (Fig. 3B, T_m, Table 1) of hybrid SANFs as compared to PCL samples. We measured a decrease in enthalpy of fusion (Fig. 3C, ΔH_m, Table 1) in the hybrid SANFs indicating less mobility of the PCL polymer chains in the presence of the protein component. Higher crystallization temperature of PCL SANFs as compared to PCL-chips (Fig. 3C, T_c, Table 1) suggests a faster crystallization rate. It is likely that the higher crystallization temperatures of the SANF scaffolds are due to polymer chain alignment induced by the high centrifugal forces of the RJS process.

3.4. Comparison with electrospun scaffolds

We reasoned that the high-voltage jet elongation and unpredictable entanglement of ensuing fibers during the electrospinning process might result in greater protein entanglement in electrospun fibers compared to RJS SANFs. To investigate this, we compared the IR spectra (between 1800 and 1500 cm^{-1}) of RJS (Fig. 4A) and electrospun (Fig. 4B) fibers over 7 days. Fiber samples

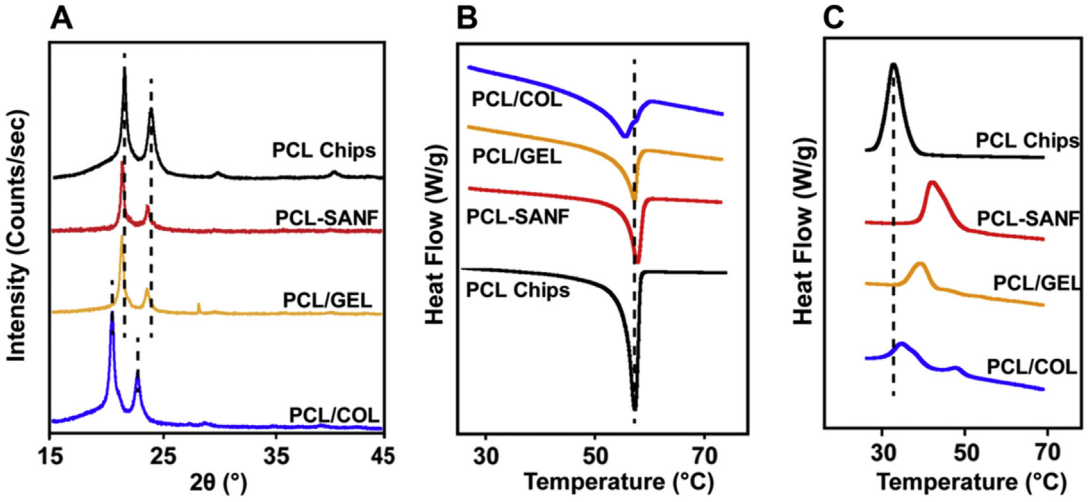

Fig. 3. Surface and thermal characterization of hybrid constructs. (A) X-ray diffraction (XRD) pattern of PCL-chips and all SANF constructs. (B) Differential Scanning Calorimetry (DSC) melting thermograms of PCL-chips and all SANF constructs. (C) DSC crystallization thermograms of PCL-chips and all SANF constructs.

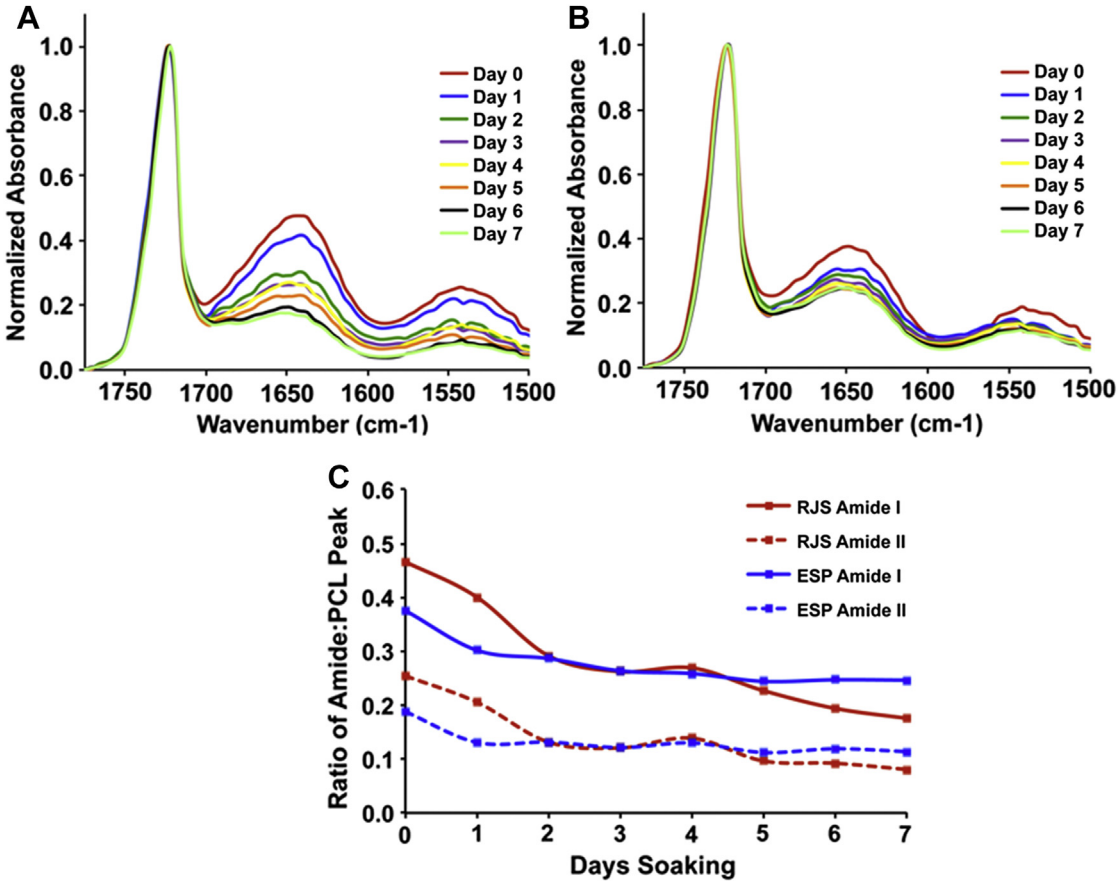

Fig. 4. Surface protein content of RJS and electrospun fibers. (A) IR spectrum of RJS fibers. (B) IR spectrum of electrospun fibers. (C) Ratio of amide I/II:PCL carbonyl peaks to quantify protein:polymer ratio in RJS and electrospun (ESP) fibers.

were kept in an aqueous environment at 37 °C between measurements to simulate *in vivo* conditions. Initially, RJS fibers had greater amounts of protein on the fiber surface as evidenced by greater Amide I:carbonyl and Amide II:carbonyl ratios (Fig. 4C). We noted a significant drop in these two ratios by day 2, suggesting that the surface proteins in RJS fibers are greater in amount and also quicker to be hydrolyzed as compared to electrospun fibers. By day 7, the surface protein content was higher in electrospun fibers compared to RJS fibers. Our results suggest greater protein-polymer entanglement and therefore slower hydrolysis of the protein component in electrospun fibers. However, RJS fibers have higher initial surface protein content, suggesting greater protein bioavailability for cell adhesion. In any case we should note that specific protein hydrolysis rates will depend on the nature of the *in vivo* milieu.

3.5. Hierarchical polymer chain alignment of SANFs

We asked if RJS induced alignment of polymer chains at the molecular scale, in addition to macroscale fiber alignment. ATR-FTIR spectra of the PCL-SANF constructs were examined by a polarized IR spectrometer when fibers positioned parallel and perpendicular to the electric vector direction of the polarizer (Supplementary Fig. 2G). Results show the typical FTIR spectra of PCL SANF in the range of 800–1800 cm^{-1} with the incident IR polarized parallel (zero degree) and perpendicular (ninety degree) to the nanofiber axis, revealing the chain orientation developed in the PCL super-aligned nanofibers produced by RJS. The intensity difference of the 1724 cm^{-1} carbonyl peak at the different polarized angles was 0.2937. The difference in ratio of amorphous (1161 cm^{-1}) to crystalline (1724 cm^{-1}) peaks at the different polarized angle was 0.3076. Taken together, these values being close to 0 suggest that most of PCL polymer chains were parallel to the nanofiber longitudinal axis.

3.6. Bioelimination and mechanical characterization

Uncrosslinked gelatin typically solubilizes in an aqueous medium, and is easily bioeliminated *in vivo* [27,28]. In order to assess if these properties were altered when blended with PCL, we quantified the rate of bioelimination of hybrid SANF scaffolds. The SANF fibers were cultured with cardiac fibroblasts in Transwell® plates (Supplementary Fig. 3A) for 2–56 days. Transwell® culture was utilized here as it allowed us to conveniently remove the scaffold for measuring scaffold dry weight while maintaining an environment that simulated biodegrading and bioeliminating conditions. Results show that after two weeks, there was no significant change in the remaining mass of the hybrid constructs for PCL/Gelatin-75/25, but dramatic and significant degradation for PCL/Gelatin-50/50 and near total dissolution of PCL/Gelatin-25/75 (Supplementary Fig. 3B). The data suggests that bioelimination of gelatin without crosslinking is protected in the PCL/Gelatin-75/25 configuration, but not in PCL/Gelatin-50/50 or PCL/Gelatin-25/75.

In order to confirm the specific degradation of the protein component of the hybrid scaffold, we analyzed the ratio of the amide II:carbonyl FTIR peaks (A:C ratio). This analysis allowed us to quantify the ratio of protein (collagen) versus polymer (PCL) within the sample as it undergoes biodegradation. We report significant reduction in the A:C ratio (Supplementary Fig. 3C) after 56 days,

suggesting loss of protein (collagen) component in the sample during biodegradation but relative stability of the polymer (i.e. PCL) component.

Mechanical anisotropy and cellular alignment is important in organs and tissues such as axonal bundles, muscle, and cardiac valves [39–41]. We measured the mechanical properties of SANF scaffolds via uniaxial mechanical testing with samples maintained at 37 °C in a PBS bath. Elastic stress-strain behavior of SANF PCL and PCL/Collagen-75/25 (Fig. 5A) showed mechanical anisotropy between the fiber (FD) and cross-fiber (X-FD) directions. Further, the Young's modulus and maximum strain of the PCL/Collagen scaffold is on the same order of magnitude as cardiac muscle and heart valve leaflets [39], suggesting their suitability for cardiovascular tissue engineering applications. In contrast, PCL constructs were an order of magnitude stiffer and had an elastic limit of 10% strain (Fig. 5A). The low extensibility of pure PCL scaffolds limits their utility in tissue engineering applications.

We also measured changes in the Young's Modulus and Ultimate Tensile Strength (UTS) of these scaffolds under the previously outlined biodegrading conditions. The Young's modulus of PCL scaffolds was not significantly altered over 56 days (Fig. 5B), while the ultimate tensile strength of PCL scaffolds was significantly decreased only after 56 days (Fig. 5C). This result was expected given the slow rate of bioresorption of PCL [42]. PCL/collagen hybrid constructs show significantly increased Young's modulus (Fig. 5D) and UTS (Fig. 5E), suggesting loss of the faster-degrading collagen component within these constructs. As a whole, these results suggest the potential use of hybrid scaffolds to increase scaffold mechanical properties over time *in vivo*.

3.7. Cell culture studies

We reasoned that the anisotropy and protein content of our SANF constructs would support the growth, development and proliferation of cells. We seeded PCL and PCL/Collagen-75/25 SANFs with cardiomyocytes, neurons and valve interstitial cells (VICs) to test this hypothesis. SEM micrographs (Fig. 6A) revealed greater cell attachment, spreading and alignment in the hybrid PCL/Collagen scaffolds as compared with the PCL scaffolds. Metabolic activity of VICs was assessed via the 3-(4,5-Dimethylthiazol-2-yl)-2,5-diphenyltetrazolium bromide (MTT) proliferation assay (Fig. 6B). Our results show that cellular metabolic activity was significantly higher on PCL/Collagen SANF constructs compared to PCL constructs after both 2 and 7 days of culture. We also assessed toxicity of the fibers via quantification of secreted lactate dehydrogenase (LDH) by cardiomyocytes seeded on SANF constructs (Fig. 6C). Cells seeded on PDMS coated glass coverslips functionalized with fibronectin were used as controls. Normalized secreted LDH after 24 h culture was statistically similar between PCL and PCL/Collagen SANF fibers and also similar to cells seeded on fibronectin functionalized PDMS coated glass coverslips, suggesting low cytotoxicity induced by these fibers.

Sarcomerogenesis in cardiomyocytes is a crucial component for cardiac contractile function [43]. We assessed myocyte sarcomerogenesis via α-actinin immunostaining (Fig. 6D). There was a greater number of striated cells in PCL/Collagen-75/25 scaffolds compared to PCL scaffolds (Fig. 6E) suggesting that hybrid scaffolds promote better sarcomere formation in cardiomyocytes compared to pure polymer scaffolds.

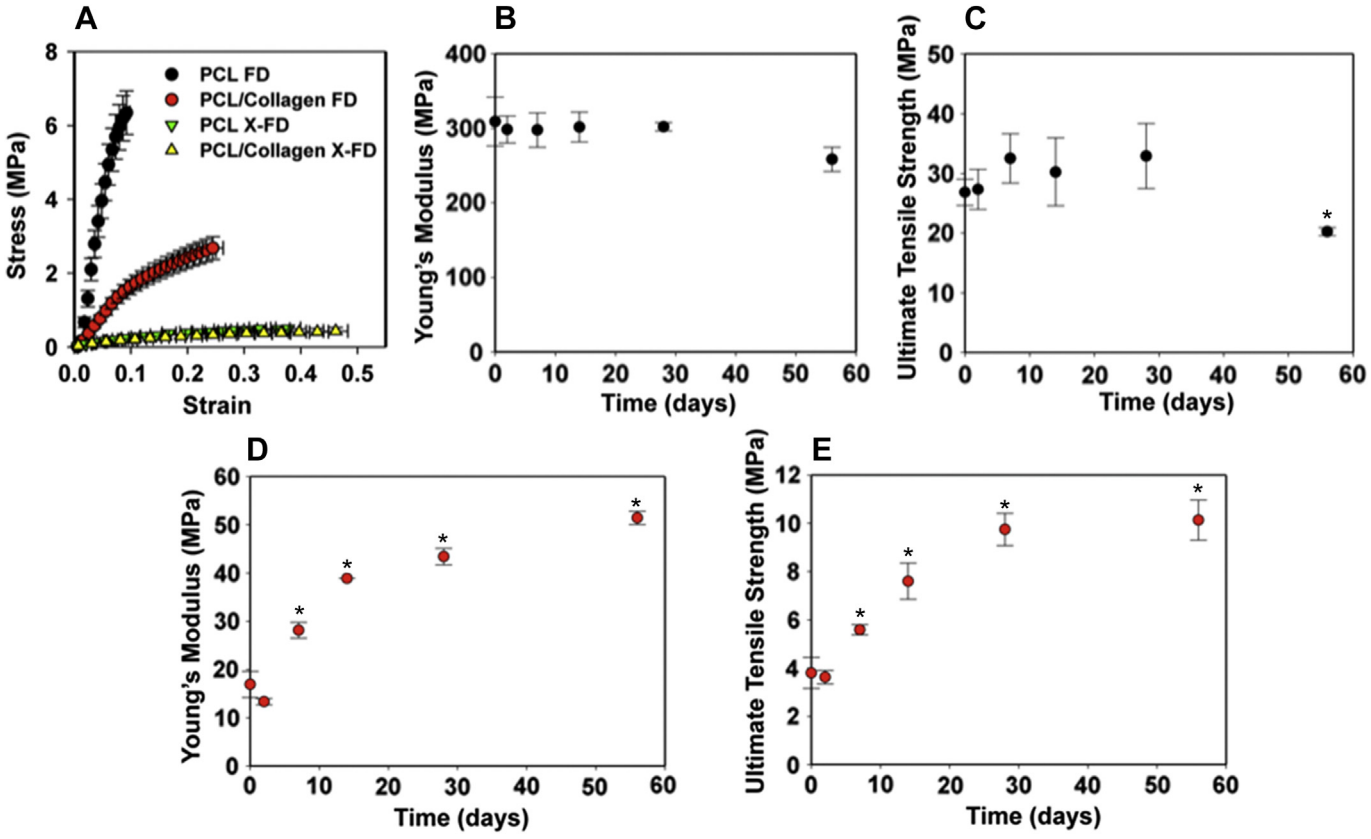

Fig. 5. Mechanical characterization of SANF constructs. (A) Stress-strain curve of the elastic regime of PCL and PCL/Collagen-75/25 SANFs. FD and X-FD denote for extension parallel to fiber direction and perpendicular to fiber direction, respectively ($N = 8$ samples). (B) Young's modulus of PCL, (C) ultimate tensile strength of PCL, (D) Young's modulus of PCL/Collagen, (E) ultimate tensile strength of PCL/Collagen SANFs over the course of the biodegradation study ($N = 4$ samples, * = statistically different from sample at day 0, $p < 0.05$). All plots: mean ± SEM.

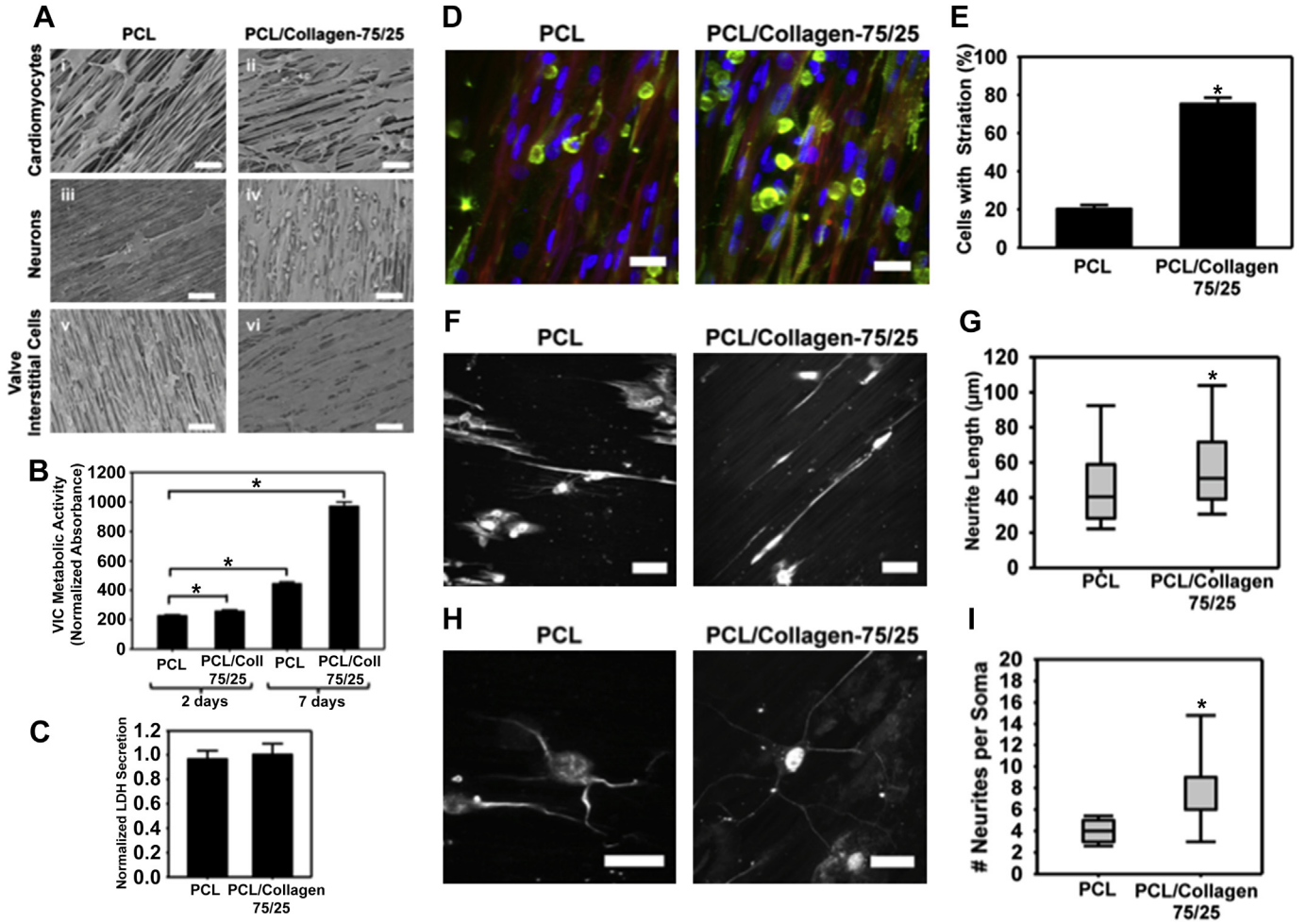

Fig. 6. Cellular culture of cardiomyocytes, cortical neurons and valve interstitial cells on SANF biohybrid constructs. (A) Representative scanning electron micrographs of PCL and PCL/Collagen-75/25 SANFs with cardiomyocytes, neurons and VICs attached to and aligning along fiber direction. Qualitatively, there are lesser cells attached to the PCL SANF constructs compared to PCL/Collagen-75/25 SANF constructs. (Scale bars: Ai, ii – 20 μm; Aiii, iv – 100 μm; Av, vi – 40 μm). (B) Cell metabolic activity assay (MTT assay) on valve interstitial cells (VICs) seeded on SANF constructs ($N = 8$, * = statistical significance at $p < 0.05$, plots = mean ± SEM). (C) Lactate dehydrogenase (LDH) cytotoxicity assay on cardiomyocytes seeded on SANF constructs compared to control ($N = 4$, plots = mean ± SEM). (D) Laser scanning confocal image of cardiomyocytes on SANF scaffolds. Cells are stained blue, α-actinin is stained green, and F-actin is stained red. (Scale bars: 25 μm) (E) Mean number of cells with striation ($N = 6$ samples with at least 8 fields of view per sample, * = statistical significance at $p < 0.05$, plots = mean ± SEM) (F) Laser scanning confocal image of cortical neurons on SANF scaffolds. Neurofilament protein is depicted in white (pseudocolor). (Scale bars: 50 μm) (G) Mean extended neurite length on PCL and PCL/Collagen-75/25 SANF ($N = 6$ samples with at least 8 fields of view per sample, * = statistical significance at $p < 0.05$; box plot: 25–75%, error bars: 10–90%) (H) Laser scanning confocal image of PCL and PCL/COL-75/25 SANF with neurite projections cells. Neurofilament protein is depicted in white (pseudocolor). (Scale bars: 20 μm) (I) Mean number of neurite projections ($N = 6$ samples with at least 8 fields of view per sample, * = statistical significance at $p < 0.05$; box plot: 25–75%, error bars: 10–90%).

We asked if SANF hybrid scaffolds permitted directed neuronal growth and maturation as these are important aspects for neural tissue engineering [44]. We assessed neurite length (Fig. 6F, G) and neurite branching (Fig. 6H, I) of primary neonatal rat neurons after 7 days in culture via immunostaining of neurofilament protein. Longer time points were not considered due to resulting overgrowth of cultures by astrocytes and glial cells. Neurite length (Fig. 6G) and branching (Fig. 6I) was significantly higher on PCL/Collagen-75/25 scaffolds compared to PCL scaffolds suggesting that the increased protein in the hybrid scaffolds provides a better environment for neuronal maturity and extension of neurite projections.

4. Discussion

The fundamental approach in tissue engineering involves the fabrication of polymeric scaffolds seeded with appropriate cells to produce a three-dimensional functional tissue suitable for *in vivo* implantation [45]. Several reports detail efforts to improve the hydrophilicity of the scaffold biotic–abiotic interface of the scaffold to promote cell adhesion and migration [46,47] via functionalization of the polymer scaffold backbone with adhesive proteins such as fibronectin, laminin or other synthetic molecules [47–49], or blending in protein with the polymer raw material to create a hybrid scaffold material [4,6,50]. Electrospinning, which is the most common method for producing nanofibers, results in scaffolds with poorer hierarchical fiber alignment which is disadvantageous when engineering anisotropic tissue types such as the heart, heart valves and tendons [6]. The current study also demonstrates key differences between electrospun and RJS fibers. We note that RJS fibers have greater protein content on the surface, which is hydrolyzed faster, due to lesser entanglement with the polymer. Therefore there may be specific applications such as those that require initial higher protein bioavailability for cell adhesion, for which RJS scaffolds will preferred over electrospun fibers.

In this study, utilizing collagen/gelatin and rotary jet spinning technology [11], we have created super-aligned hybrid nanofiber scaffolds that can be used for a wide variety of tissue engineering applications. Data suggests that a 75/25-polymer/protein ratio imparts biomimeticity to the scaffold without compromising its physical, mechanical and biodegradation properties. Previous studies [6,51] have used up to 50/50-polymer/protein blends, but we observed significant increase in fiber diameter, reduction in alignment and increased biodegradation rate at protein concentrations of 50% and above. Higher rotational speeds (above 30,000 rpm) during RJS SANF fabrication can be used to reduce the fiber diameter and force better alignment, but the effect of increased shear forces due to higher rotational speeds on protein denaturation and unfolding has not been fully characterized [17].

Cells cultured on these hybrid SANF scaffolds show highly aligned morphologies and improved cellular proliferation and viability over pure polymer SANF scaffolds. Additionally, the alignment of these fibers promoted striation in cardiomyocytes, proliferation in VICs, as well as directed neurite projections and branching in primary cortical neurons. Future studies will seek to evaluate the long-term viability of these scaffolds *in vivo*.

5. Conclusion

We report the fabrication of rotary jet spun biohybrid PCL/gelatin and PCL/collagen nanofibers that have an extremely high degree of alignment. We demonstrate that the physical, chemical and mechanical properties of these super-aligned nanofibers (SANF) are dependent on the percentage composition of protein in these fibers. PCL/collagen-75/25 SANF scaffolds were selected for cell culture study as that composition provided better mechanical and biodegradation properties compared to other hybrid or pure polymer compositions. Cell culture results demonstrated better cell attachment, proliferation and function on SANF hybrid fibers, suggesting their potential utility in tissue engineering applications.

Acknowledgments

We acknowledge support from Harvard Materials Research Science and Engineering Center (MRSEC) award number DMR-0213805, Harvard Center for Nanoscale Systems (CNS) for use of equipment, and the Wyss Institute for Biologically Inspired Engineering. We acknowledge our partnership with the Sogang-Harvard Center for Disease Biophysics Research. We thank Patrick Campbell and Matthew Hemphill for assisting with cell culture experiments. H.M.G. acknowledges the National Science Foundation Graduate Research Fellowship Program.

Appendix A. Supplementary data

Supplementary data related to this article can be found at http://dx.doi.org/10.1016/j.biomaterials.2013.12.072.

References

[1] Langer R, Vacanti JP. Tissue engineering. Science 1993;260:920–6.
[2] Vacanti JP, Langer R. Tissue engineering: the design and fabrication of living replacement devices for surgical reconstruction and transplantation. Lancet 1999;354(Suppl 1):SI32–4.
[3] Hutmacher DW. Scaffold design and fabrication technologies for engineering tissues–state of the art and future perspectives. J Biomater Sci Polym Ed 2001;12:107–24.
[4] Urciuolo F, Imparato G, Guaccio A, Mele B, Netti PA. Novel strategies to engineering biological tissue in vitro. Methods Mol Biol 2012;811:223–44.
[5] Ma Z, He W, Yong T, Ramakrishna S. Grafting of gelatin on electrospun poly(caprolactone) nanofibers to improve endothelial cell spreading and proliferation and to control cell orientation. Tissue Eng 2005;11:1149–58.
[6] Ghasemi-Mobarakeh L, Prabhakaran MP, Morshed M, Nasr-Esfahani MH, Ramakrishna S. Electrospun poly(epsilon-caprolactone)/gelatin nanofibrous scaffolds for nerve tissue engineering. Biomaterials 2008;29:4532–9.
[7] Powell HM, Boyce ST. Engineered human skin fabricated using electrospun collagen-PCL blends: morphogenesis and mechanical properties. Tissue Eng Part A 2009;15:2177–87.
[8] Levy RJ, Schoen FJ, Levy JT, Nelson AC, Howard SL, Oshry LJ. Biologic determinants of dystrophic calcification and osteocalcin deposition in glutaraldehyde-preserved porcine aortic valve leaflets implanted subcutaneously in rats. Am J Pathol 1983;113:143–55.
[9] Webb CL, Nguyen NM, Schoen FJ, Levy RJ. Calcification of allograft aortic wall in a rat subdural model. Pathophysiology and inhibition by Al3+ and aminodiphosphonate preincubations. Am J Pathol 1992;141:487–96.
[10] Chong EJ, Phan TT, Lim IJ, Zhang YZ, Bay BH, Ramakrishna S, et al. Evaluation of electrospun PCL/gelatin nanofibrous scaffold for wound healing and layered dermal reconstitution. Acta Biomater 2007;3:321–30.
[11] Badrossamay MR, McIlwee HA, Goss JA, Parker KK. Nanofiber assembly by rotary jet-spinning. Nano Lett 2010;10:2257–61.
[12] Weitz RT, Harnau L, Rauschenbach S, Burghard M, Kern K. Polymer nanofibers via nozzle-free centrifugal spinning. Nano Lett 2008;8:1187–91.
[13] Arumuganathar S, Jayasinghe SN. Living scaffolds (specialized and unspecialized) for regenerative and therapeutic medicine. Biomacromolecules 2008;9:759–66.
[14] Greiner A, Wendorff JH. Electrospinning: a fascinating method for the preparation of ultrathin fibers. Angew Chem 2007;46:5670–703.
[15] Nijst CL, Bruggeman JP, Karp JM, Ferreira L, Zumbuehl A, Bettinger CJ, et al. Synthesis and characterization of photocurable elastomers from poly(-glycerol-co-sebacate). Biomacromolecules 2007;8:3067–73.
[16] Yi F, LaVan DA. Poly(glycerol sebacate) nanofiber scaffolds by core/shell electrospinning. Macromol Biosci 2008;8:803–6.
[17] Mellado P, McIlwee HA, Badrossamay MR, Goss JA, Mahadevan L, Parker KK. A simple model for nanofiber formation by rotary jet-spinning. Appl Phys Lett 2011;99.
[18] Boland ED, Pawlowski KJ, Barnes CP, Simpson DG, Wnek GE, Bowlin GL. Electrospinning of bioresorbable polymers for tissue engineering scaffolds. Acs Sym Ser 2006;918:188–204.
[19] Kweon H, Yoo MK, Park IK, Kim TH, Lee HC, Lee HS, et al. A novel degradable polycaprolactone networks for tissue engineering. Biomaterials 2003;24:801–8.
[20] Di Lullo GA, Sweeney SM, Korkko J, Ala-Kokko L, San Antonio JD. Mapping the ligand-binding sites and disease-associated mutations on the most abundant protein in the human, type I collagen. J Biol Chem 2002;277:4223–31.
[21] Sell SA, McClure MJ, Garg K, Wolfe PS, Bowlin GL. Electrospinning of collagen/biopolymers for regenerative medicine and cardiovascular tissue engineering. Adv Drug Deliv Rev 2009;61:1007–19.
[22] Zhang Y, Ouyang H, Lim CT, Ramakrishna S, Huang ZM. Electrospinning of gelatin fibers and gelatin/PCL composite fibrous scaffolds. J Biomed Mater Res B Appl Biomater 2005;72:156–65.
[23] Choi JS, Lee SJ, Christ GJ, Atala A, Yoo JJ. The influence of electrospun aligned poly(epsilon-caprolactone)/collagen nanofiber meshes on the formation of self-aligned skeletal muscle myotubes. Biomaterials 2008;29:2899–906.
[24] Bray DF, Bagu J, Koegler P. Comparison of hexamethyldisilazane (HMDS), Peldri II, and critical-point drying methods for scanning electron microscopy of biological specimens. Microsc Res Tech 1993;26:489–95.
[25] Hamley IW. Introduction to soft matter: polymers, colloids amphiphiles, and liquid crystals. Chichester New York: Wiley; 2000.
[26] Volfson D, Cookson S, Hasty J, Tsimring LS. Biomechanical ordering of dense cell populations. Proc Natl Acad Sci USA 2008;105:15346–51.
[27] Kai D, Prabhakaran MP, Stahl B, Eblenkamp M, Wintermantel E, Ramakrishna S. Mechanical properties and in vitro behavior of nanofiber-hydrogel composites for tissue engineering applications. Nanotechnology 2012;23:095705.
[28] Peng Y, Ang M, Foo S, Lee WS, Ma Z, Venkatraman SS, et al. Biocompatibility and biodegradation studies of subconjunctival implants in rabbit eyes. PLoS One 2011;6:e22507.
[29] Geisse NA, Sheehy SP, Parker KK. Control of myocyte remodeling in vitro with engineered substrates. Vitro Cell Dev Biol Anim 2009;45:343–50.
[30] Hemphill MA, Dabiri BE, Gabriele S, Kerscher L, Franck C, Goss JA, et al. A possible role for integrin signaling in diffuse axonal injury. PLoS One 2011;6:e22899.
[31] Feinberg AW, Feigel A, Shevkoplyas SS, Sheehy S, Whitesides GM, Parker KK. Muscular thin films for building actuators and powering devices. Science 2007;317:1366–70.
[32] Balachandran K, Alford PW, Wylie-Sears J, Goss JA, Grosberg A, Bischoff J, et al. Cyclic strain induces dual-mode endothelial-mesenchymal transformation of the cardiac valve. Proc Natl Acad Sci USA 2011;108:19943–8.
[33] Grosberg A, Kuo PL, Guo CL, Geisse NA, Bray MA, Adams WJ, et al. Self-organization of muscle cell structure and function. PLoS Comput Biol 2011;7:e1001088.
[34] Zeugolis DI, Khew ST, Yew ES, Ekaputra AK, Tong YW, Yung LY, et al. Electrospinning of pure collagen nano-fibres – just an expensive way to make gelatin? Biomaterials 2008;29:2293–305.
[35] Payne KJ, Veis A. Fourier transform IR spectroscopy of collagen and gelatin solutions: deconvolution of the amide I band for conformational studies. Biopolymers 1988;27:1749–60.

[36] Muyonga JH, Cole CGB, Duodu KG. Fourier transform infrared (FTIR) spectroscopic study of acid soluble collagen and gelatin from skins and bones of young and adult Nile perch (Lates niloticus). Food Chem 2004;86:325–32.
[37] Coleman MM, Zarian J. Fourier-transform infrared studies of polymer blends. II. poly(epsilon-caprolactone)-poly(vinyl chloride) system. J Polym Sci 1979;17:837–50.
[38] Gupta KK, Kundan A, Mishra PK, Srivastava P, Mohanty S, Singh NK, et al. Polycaprolactone composites with TiO2 for potential nanobiomaterials: tunable properties using different phases. Phys Chem Chem Phys 2012;14:12844–53.
[39] Sacks MS, David Merryman W, Schmidt DE. On the biomechanics of heart valve function. J Biomech 2009;42:1804–24.
[40] Maganaris CN, Paul JP. Tensile properties of the in vivo human gastrocnemius tendon. J Biomech 2002;35:1639–46.
[41] Mathur AB, Collinsworth AM, Reichert WM, Kraus WE, Truskey GA. Endothelial, cardiac muscle and skeletal muscle exhibit different viscous and elastic properties as determined by atomic force microscopy. J Biomech 2001;34:1545–53.
[42] Sinha VR, Bansal K, Kaushik R, Kumria R, Trehan A. Poly-epsilon-caprolactone microspheres and nanospheres: an overview. Int J Pharm 2004;278:1–23.
[43] Bursac N, Parker KK, Iravanian S, Tung L. Cardiomyocyte cultures with controlled macroscopic anisotropy: a model for functional electrophysiological studies of cardiac muscle. Circ Res 2002;91:e45–54.
[44] Hoffman-Kim D, Mitchel JA, Bellamkonda RV. Topography, cell response, and nerve regeneration. Annu Rev Biomed Eng 2010;12:203–31.
[45] Khademhosseini A, Vacanti JP, Langer R. Progress in tissue engineering. Sci Am 2009;300:64–71.
[46] Li WJ, Cooper Jr JA, Mauck RL, Tuan RS. Fabrication and characterization of six electrospun poly(alpha-hydroxy ester)-based fibrous scaffolds for tissue engineering applications. Acta Biomater 2006;2:377–85.
[47] Cao B, Yan S, Zhang K, Song Z, Cao T, Chen X, et al. A poly(acrylic acid)-block-poly(L-glutamic acid) diblock copolymer with improved cell adhesion for surface modification. Macromol Biosci 2011;11:970–7.
[48] Desmet T, Poleunis C, Delcorte A, Dubruel P. Double protein functionalized poly-epsilon-caprolactone surfaces: in depth ToF-SIMS and XPS characterization. J Mater Sci Mater Med 2012;23:293–305.
[49] Rosellini E, Barbani N, Giusti P, Ciardelli G, Cristallini C. Molecularly imprinted nanoparticles with recognition properties towards a laminin H-Tyr-Ile-Gly-Ser-Arg-OH sequence for tissue engineering applications. Biomed Mater 2010;5:065007.
[50] Schumann D, Ekaputra AK, Lam CX, Hutmacher DW. Biomaterials/scaffolds. Design of bioactive, multiphasic PCL/collagen type I and type II-PCL-TCP/collagen composite scaffolds for functional tissue engineering of osteochondral repair tissue by using electrospinning and FDM techniques. Methods Mol Med 2007;140:101–24.
[51] Ghasemi-Mobarakeh L, Prabhakaran MP, Morshed M, Nasr-Esfahani MH, Ramakrishna S. Bio-functionalized PCL nanofibrous scaffolds for nerve tissue engineering. Mat Sci Eng C-Mater 2010;30:1129–36.